Iranian Journal of Analytical Chemistry
Volume 6, Issue 1, March 2019 (38-48)

مجله ایرانی شیمی تجزیه
دوره۶، شماره ۱، فروردین ماه ۱۳۹۸ (۴۸-۳۸)

نظارت تصویری بر فساد مواد غذایی توسط بیوسنسور ساخته‌شده از نانوذرات طلا ساپورت‌شده بین فسفسیلیکات فیبری

سید محسن صادق زاده[۱و۲*]، راحله ژیانی[۱و۲]، علی اسحاقی[۳]
۱. باشگاه پژوهشگران و نخبگان جوان، دانشگاه آزاد اسلامی واحد نیشابور، خراسان رضوی ، ایران
۲. مرکز تحقیقات تکنولوژی مواد و پردازش مواد جدید، گروه شیمی، دانشگاه آزاد اسلامی واحد نیشابور، خراسان رضوی، ایران
۳. گروه زیست شناسی، دانشگاه آزاد اسلامی واحد مشهد، خراسان رضوی ، ایران
تاریخ دریافت: ۹ بهمن ۱۳۹۷ تاریخ پذیرش: ۲۹ اسفند ۱۳۹۷

Visual Monitoring of Food Spoilage Based on Hydrolysis-Induced Mercury Metallization of New Gold Nanoparticles Between Fibrous Phosphosilicate

Seyed Mohsen Sadeghzadeh[*,1,2], Rahele Zhiani [1,2], Ali Es-haghi[3]
1. Young Researchers and Elite Club, Neyshabur Branch, Islamic Azad university, P.O. Box 97175-613, Neyshabur, Iran
2. New Materials Technology and Processing Research Center, Department of Chemistry, Neyshabur Branch, Islamic Azad University, Neyshabur, Iran
3. Department of Biology, Mashhad Branch, Islamic Azad University, Mashhad, Iran
Received: 29 January 2019 **Accepted:** 20 March 2019
DOI: 10.30473/ijac.2019.44117.1139

چکیده
زباله‌های مواد غذایی یکی از مسائل اصلی برای جوامع بین‌المللی است. این فقط یک مسئله اخلاقی و اقتصادی نیست، بلکه منابع طبیعی محدود را نیز کاهش می‌دهد. در میان استراتژی‌های مناسب برای مبارزه با چنین چالشی، بسته‌بندی هوشمند یک ابزار جالب برای کاهش ضایعات ناشی از خانواده‌ها و خرده‌فروشان است. تشخیص رنگ‌سنجی آمین‌های بیوژنیک، معیارهای شناخته‌شده فساد مواد غذایی، نقش اصلی نظارت بر ایمنی مواد غذایی را نشان می‌دهد. یک سنسور رنگی جدید بر اساس واکنش فلزسازی جیوه ناشی از هیدرولیز رزونانس پلاسمون سطحی بر روی نانوذرات طلا حساس به نیتروژن فرار آزادشده از گوشت برای نظارت بر کیفیت گوشت در زمان مصرف سنتز شد. سنسورها در فضایی شبیه‌سازی آمونیاک نگهداری شدند که تغییر رنگ آن را با تغییر pH تغییر دادند. این آمین‌های بسیار فرار توسط مواد غذایی خراب‌شده، به ویژه گوشت فاسد تولید می‌شود، که باعث تغییر رنگ برچسب‌های هوشمند می‌شوند که می‌توان به عنوان یک تست بصری برای طراوت مواد غذایی استفاده شود.

واژه‌های کلیدی
شیمی سبز؛ بیوسنسور؛ آمین‌های بیوژنیک؛ کموسنسور؛ غذای بسته بندی شده؛ نانوذرات.

Abstract
Food waste is one of the main issues for international organisms. It is not only an ethical and economic issue but it also depletes the environment of limited natural resources. Among strategies suitable for fighting such challenge, intelligent packaging is an interesting tool to reduce waste derived from households and retailers. Colorimetric detection of biogenic amines, well-known criterions of food corruption, shows the main role for monitoring of food safety. A novel colorimetric sensor based on hydrolysis-induced mercury metallization reaction to tune the localized surface plasmon resonance (LSPR) adsorption of Au nanoparticles sensitive to total volatile basic nitrogen (TVBN) released from meat has been created for real-time supervision of meat quality. Sensors were kept in atmosphere of ammonia simulating which changed its colour with changing of pH. This is the case of highly volatile amines, produced in food spoilage, specifically in the deterioration of meat, for which the color development of the smart labels can be used as a visual test for food freshness.

Keywords
Green Chemistry; Biosensor**;** Biogenic Amines; Chemosensors; Packaged Food; Nanoparticle.

*Corresponding Author: seyedmohsen.sadeghzadeh@gmail.com

1. INTRODUCTION

Food waste is one of the basic problems for humane society that the concern is growing in most of the countries. Recently, due to environmental problems, diseases and hunger created in the international community, a massive effort has been made to reduce food waste. One of the stages in the production of food waste is uncertain food storage and unsuitable packaging. Food packaging is an essential medium for preserving food quality and prolongs the shelf life of food products, hence potentially reducing wasted food and its environmental impacts. In addition, an appropriate package can play a significant role in food security and safety, and subsequently, reduce funding for the production and therapy. Intelligent packaging is a new technique in the field of food packaging, which it informs about the status of the food and its storage conditions. In recent years, there have been significant advances in sensors, colorimetric sensors, and biosensor. However, this technology is utilized to investigate the quality and safety as well as sense the spoilage in food products by monitoring the changes in chemical and physical properties [1-5].

Colorimetric sensors are especially appealing for in applications. Colorimetric sensors are usually simple and cheap, and can be directly read out by naked eyes. Over the past decade, they have been developed for the diagnosis of biogenic amines. It is noteworthy, they suffer from low color clarity by using complicated design and intricate output or single chromogenic reagent by using multiple chromogenic reagents for the end-users [6-9]. In recent research, various biosensor to tune the LSPR adsorption of gold NRs have been suggested for visual detection of alkaline phosphatase activity,[10] prostatespecific antigen,[11] human immunoglobulin G,[12] bacteria [13]. However, these biosensors have limitations with respect to the cost and stability due to the usage of bioenzymes. Guo and colleagues reported a simple and effective method for visual monitoring of biogenic amines to in situ evaluate food freshness and spoilage by naked eyes with high color resolution. The principle of this method was based on the integration of hydrolysis-induced silver metallization by biogenic amines with the fascinating LSPR property of Au NRs [14].

Meat is one of the foods with a wide range of food products. If they are not properly stored and packaged, they quickly deteriorate [15, 16]. Meat products are naturally decomposed and contain high fat and water [17, 18]. Such products are both sensitive to destroy with both lipid oxidation and microbial contamination [19]. The split meat is dangerous because of the microbial growth and consequently the distribution of food born diseases [20]. Typically, sensory evaluation, chemical testing, including the evaluation of microbial growth, are two key methods for assessing the quality of meat degradation [21-23]. In the usual meat sensory evaluation, properties such as color, taste, adhesion, and elasticity of the tissue can be used. Biogenic amines (BA) are important volatile organic compounds (VOCs) which are mainly produced by decarboxylation of amino acids, or by amination and transamineation of aldehydes and ketones in several foods, such as fish, meat, cheese, vegetables, and wine [24]. The production of biogenic amines can happen as the processing and storage of food as a result of bacterial activity [25, 26]. The use of low-quality raw materials, inappropriate conditions of processing and maintenance, and microbial contamination lead to an increase in the level of certain amines [27-30]. From the toxicological point of view, the presence of BA in foods can lead to nerve, gastrointestinal and allergic disorders illnesses, whose removal and monitoring methods of BA can play a significant role in health [31]. In addition, the number of amino acids can be used as a quality control agent for fresh food [32-34]. Here we hypothesized that, by putting up gold NPs between fibrous phosphosilicate (FPS) fibers through obstruction of FPS by β-cyclodextrin (βCD) through a stimuli-sensitive bond via the interface carbonyldiimidazole (CDI) (e.g., an pH responsive bond), one is able to not only load gold NPs between FPS fibers but also control gold release kinetics from the NPs. Also, we proposed a universal steady hydrolysis-induced mercury metallization reaction by basic biogenic amines to tune the localized surface plasmon resonance adsorption peak of Hg (II) complex (Fig. 1).

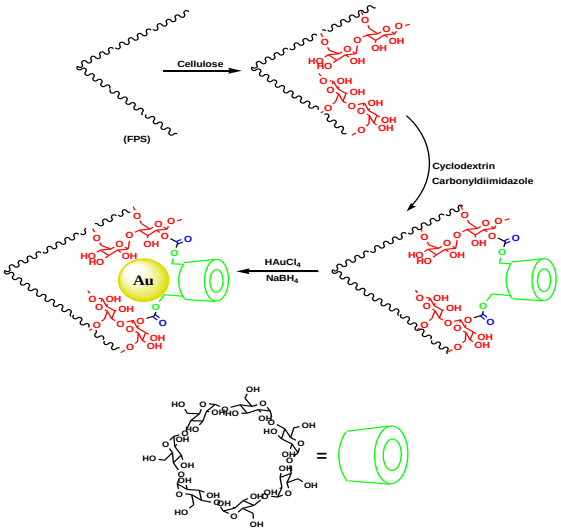

Fig. 1. Schematic description of the synthesis of FPS/βCD/Au NPs.

2. EXPERIMENTAL

2.1. Materials and Methods

Chemical materials were purchased from Fluka and Merck in high purity. Melting points were determined in open capillaries using an Electrothermal 9100 apparatus and are uncorrected. FTIR spectra were recorded on a VERTEX 70 spectrometer (Bruker) in the transmission modein spectroscopic grade KBr pellets for all the powders. The particle size and structure of nano particle was observed by using a Philips CM10 transmission electron microscope operating at 100 kV. Powder X-ray diffraction data were obtained using Bruker D8 Advance model with Cu ka radition. The thermogravimetric analysis (TGA) was carried out on a NETZSCH STA449F3 at a heating rate of 10 °C min^{-1} under nitrogen. ^{1}H and ^{13}C NMR spectra were recorded on a BRUKER DRX-300 AVANCE spectrometer at 300.13 and 75.46 MHz, BRUKER DRX-400 AVANCE spectrometer at 400.22 and 100.63 MHz, respectively. Elemental analyses for C, H, and N were performed using a Heraeus CHN–O-Rapid analyzer. The purity determination of the products and reaction monitoring were accomplished by TLC on silica gel polygram SILG/UV 254 plates. Mass spectra were recorded on Shimadzu GCMS-QP5050 Mass Spectrometer.

2.2. General procedure for the preparation of ligand *DFA/CS_2/Hg(II) NPs*

Diphenylamine (DFA) (4 mmol) and carbon disulphide (4 mmol) were dissolved in ethanol (20 mL) and stirred for 30 min at 5 °C. $HgCl_2$ (2.0 mmol) was dissolved in 20 mL of water and added to the solution. A pale yellow powder precipitated, which was filtered and dried [35].

2.3. General procedure for the preparation of FPS

Tetraethyl orthosilicate (TEOS) (2.08 g) and tripolyphosphate (TPP) (3.67 g) were dissolved in a solution of cyclohexane (30 mL) and 1-pentanol (1.5 mL). A stirred solution of cetylpyridinium bromide (CPB) (1 g) and urea (0.5 g) in water (30 mL) was then added to the top mixture. The resulting mixture was continually stirred for 45 min at room temperature and then placed in a teflon-sealed hydrothermal reactor and heated at 120 °C for 5 h. The FPS was then isolated by centrifugation, washed with deionized water and acetone, and dried in a drying oven [36].

2.4. General procedure for the preparation of cellulose-FPS NPs

FPS (50 mg) and water (20 mL) were mixed together in a beaker, and then acetic acid (0.75 mL) was dispersed in to the mixture by ultrasonication. Cellulose (250 mg) was added at room temperature and stirred for another 16 h at 60 °C. The resultant products were collected and washed with ethanol and deionized water in sequence, and then dried under vacuum at 60 °C for 2 h for further use [36].

2.5. General procedure for the preparation of cellulose-FPS/βCD NPs

βCD (0.10 mmol) was dissolved in DMSO (3 mL) and Triethylamine (60 µL, 81.0 mg, 0.80 mmol) was added. The flask was purged with argon and then solid 1,1'-Carbonyldiimidazole (CDI) (0.8 mmol) was added. The mixture was stirred at room temperature for 5 hours under argon atmosphere. In the meantime, cellulose-FPS (40 mg) was dispersed in distilled water (15 mL) by sonication for 1 h. A solution of activated βCD was added to the dispersion of cellulose-FPS. The reaction mixture was sonicated for 8 h, followed by shaking (250 rpm) at room temperature overnight. The obtained suspension was transferred to the centrifuge tube. The tube was centrifuged (5000 rpm, 25 min, 24 °C). The supernatant was separated from the carbon material. The residue was then sonicated with distilled water (35 mL) at 24 °C for 20 min. The resulting product was dried with the help of vacuum at 75°C.

2.6. General procedures for preparation of the FPS/βCD/Au NPs

FPS/βCD (200 mg) and $HAuCl_4.3H_2O$ solution (10 mM, 2.67 mL, 0.027 mmol) was added into the suspension under continuous stirring and the mixture was continually stirred for 1 h at room temperature. Subsequently, fresh, ice-cold $NaBH_4$ solution (30 mM, 2.67 mL, 0.080 mmol) was delivered dropwise to the above suspension. The color of the solution rapidly changed to red. The obtained solid material was isolated by centrifugation, washed repeatedly with deionized water and ethanol, and dried overnight under vacuum at 30 °C [36].

2.7. The fabrication method of the sensory material

Conical snap cap polypropylene microcentrifuge tubes (1.5 mL in size) were used to prepare the portable sensory hydrogels. Agarose (20 mg) was completely dissolved in boiling water (2 mL) with stirring. When the solution was cooled down to 40 °C, 200 µL of concentrated FPS/βCD/Au NPs solution, 30 µL of RMA ethanol solution (25%, w/w) and 20 µL of DFA/CS_2/Hg(II) NPs (50 mmol L^{-1}) were added and homogenized. The mixture solution (100 µL) was transferred into the

inside of snap cap of microcentrifuge tube. The sensory hydrogel was solidified after 5 min under ambient temperature [14].

3. RESULT AND DISCUSSION

The measurement mechanism for visual recognition of biogenic amines was shown in Fig. 2. After volatile biogenic amines produced during food storage percolate into the sensory hydrogels, which are created by solidifying the measurement materials consisting of FPS/βCD/Au NPs, and DFA/CS_2/Hg(II) in agarose hydrogel, and raise the pH in the hydrogel.

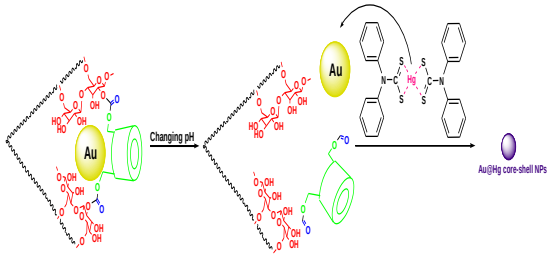

Fig. 2. Schematic illustrations of the structure of FPS-gold, the formation of FPS/βCD/Au NPs and sensing mechanism of hydrolysis-Induced mercury metallization on the surface of Au NPs by volatile biogenic amines for monitoring of food spoilage.

TEM and FESEM images of FPS are shown in Fig. 3. It can be found that the FPS sample consists of wall-like domains (Fig. 3a) and the wall sizes are fixed (Fig. 3d). Close inspection of these images reveals that the material possesses dendrimeric fibers (thicknesses of 8–10 nm) arranged in three dimensions to form walls, which can allow easy access to the available high surface area. To study the effect of the silica and phosphate concentration on the morphology, we conducted a series of experiments in which TPP-to-TEOS molar ratios were varied. When equal amounts of TEOS and TPP were used, the FPSs were monodispersed thin fibers with a single-handed wall. The FESEM and TEM images of cellulose-FPS/βCD NPs showed that after modification the morphology of FPS is not change (Figures 3b and 3e). The fibers of FPS has many Si–OH and P–OH groups on the surfaces. The Si–OH and P–OH groups on the surface could serve as aggregation centers for the growth of Au NPs on the surface of FPS. Fig. 3c and 3f shows a FESEM and TEM image of the Au NPs. As we can see, the as-prepared metal nanoparticles are spherical without obvious aggregation. The diameter of the Au NPs was about 20-40 nm, and the morphology of the NPs is near-wall (Figures 3c and 3f).

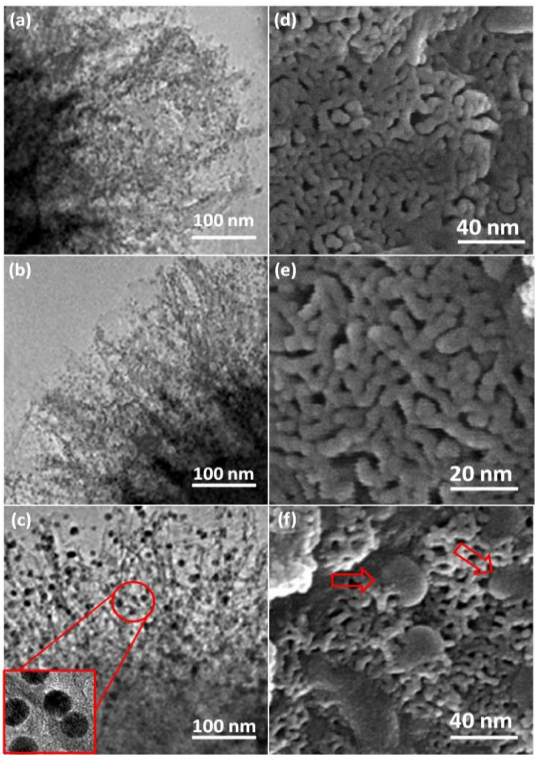

Fig. 3. TEM images of FPS NPs (a); cellulose-FPS/βCD NPs (b); FPS/βCD/Au NPs (c); FESEM images of FPS NPs (d); cellulose-FPS/βCD NPs (e); and FPS/βCD/Au NPs (f).

The XRD pattern of FPS and FPS/βCD/Au NPs is shown in Fig. 4. The XRD pattern of FPS NPs displays a number of crystalline peaks, consistent with a similar reports (Fig. 4a) [37]. Moreover, new peaks at 2θ = 38.1°, 44.3°, 64.5°, and 77.7° reflection of Au (JCPDS 04-0784) (Fig. 4b) crystal were observed for FPS/βCD/Au NPs confirming the successful growth of Au particles on the surface of cellulose-FPS/βCD again. The broad peak between 20–30° corresponds to amorphous silica. XRD analysis can easily indexed to the cubic phase of Au NPs. Fig. 4b reveals that Au NPs exhibit sharp peaks of Au (111), Au (200), Au (220), Au (311), and Au (222).

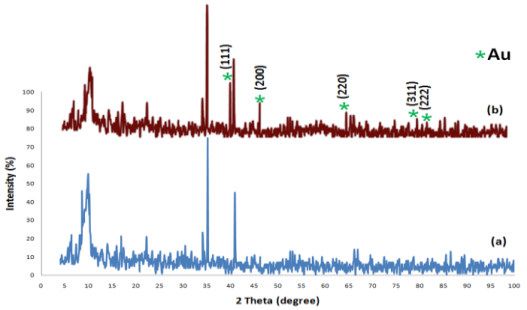

Fig. 4. XRD analysis of (a) FPS NPs, and (b) cellulose-FPS/βCD NPs.

The thermal behavior of FPS/βCD/Au NPs is shown in Fig. 5. The weight loss below 150 ºC was ascribed to the elimination of the physisorbed and chemisorbed solvent on the surface of the FPS/βCD/Au NPs material. In the second stage (180–350 ºC), weight loss is about 29 wt% for al of catalysts, which can be attributed to the cellulose and βCD as a organic group derivatives. Decrease in weight at this temperature may be rationalized by oxidation of cellulose and βCD at around 180–350 ºC. In fact, the remaining mass after the organic decomposition in FPS/βCD/Au NPs is due to the FPS and Au NPs.

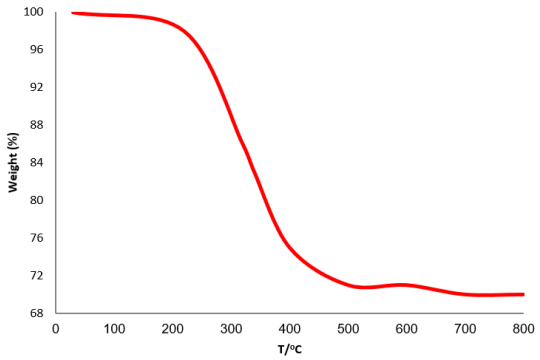

Fig. 5. TGA diagram of FPS/βCD/Au NPs.

The representative FT-IR spectrum of FPS and FPS/βCD/Au and presented in Fig. 6. The FT-IR analyzes of FPS represent the following functional groups. The pure FPS showed a typical broad peak around 3399 cm^{-1} associated with the presence of hydroxyl groups and the intensity of this peak increased which could be due to the presence of immobilized phosphate group on the framework of the FPS. The FPS materials also showed additional peak around 1483 cm^{-1} which is ascribed to the phosphate moiety coming from TPP [38]. The main peak in the spectrumof FPS is the additional peak appeared at 1232 cm^{-1}, which could be assigned to the -P=O stretching vibration indicating the presence of phosphate group [39,40]. The band at 963 cm^{-1} and the shoulder at 1108 cm^{-1} are due to the TO and LO modes of asymmetric stretching of Si-O-P bonds, respectively [41,42]. The band at about 724, and 795 cm^{-1} were assigned to the asymmetric stretching of the bridging oxygen atoms bonded to a phosphorus atom [43]. These peaks suggested successful reaction between the TEOS and the TPP (Fig. 6a). These clearly indicate the grafting of organic compound on the surface of FPS. The FPS/βCD/Au composite shows bands at around 1091, 793 and 462 cm^{-1}. A strong and broad absorption band at 3000-3550 cm^{-1} is related to the -OH stretching vibrations and two narrow peaks at around 2930 cm^{-1} are assigned to -CH fragments. The characteristic absorption bands coming from the O-C-O moiety in βCD (1120-1075 cm^{-1}) are observed in the spectrum of material FPS/βCD/Au. Importantly, the absorption band at ca. 1725–1690 cm^{-1} is ascribed to the carbamate-type linkage between cellulose and βCD (Fig. 6b).

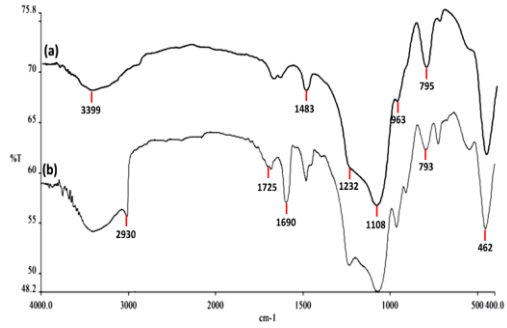

Fig. 6. FTIR spectra of (a) FPS NPs, and (b) FPS/βCD/Au NPs.

As for FPS, the BET surface area, total pore volume, and BJH pore diameter are obtained as 34 m^2/g, 0.24 cm^3/g, and 2.43 nm, whereas the corresponding parameters of cellulose-FPS/βCD have decreased to 26 m^2/g, 0.17 cm^3/g, and 1.93 nm. The nitrogen sorption analysis of CS-FPS also confirms a regular and uniform mesostructure with a decrease in surface area, pore diameter and pore volume parameters in comparison with that of pristine FPS. With the functionalization by CS, the corresponding pore volumes are drastically reduced. This could be ascribed to increased loading with the sensing probe, which occupies a large volume inside the phosphosilicat walls. The formation of Au nanoparticles upon reduction led to further, and reduction of the porosity properties (Table 1, entry 3). The formation of Au nanoparticles upon reduction led to further, but less pronounced, reduction of the porosity properties. Interestingly, in the case of FPS/βCD/Au the reduction of pore volume upon the formation of particles was particularly marked (from 0.17 cm^3g^{-1} of cellulose-FPS/βCD to 0.09 cm^3g^{-1} of FPS/βCD/Au). This finding suggests the formation of Au nanoparticles directly within the pores of the cellulose-FPS/βCD derivative (Table 1).

Table 1. Structural parameters of FPS, cellulose-FPS/βCD, and FPS/βCD/Au materials determined from nitrogen sorption experiments.

Catalysts	S_{BET} (m^2 g^{-1})	V_t (cm^3 g^{-1})	D_{BJH} (nm)
FPS	34	0.24	2.43
cellulose-FPS/βCD	26	0.17	1.93
FPS/βCD/Au	13	0.09	1.05

To verify this sensing mechanism, diethanolamine (DEA) was first used to mimick biogenic amines to mercury metallization on the Au NPs. The spectra of the UV–vis absorption is shown in Fig. 7, the solution color is ruby red and a band of Au NPs is observed in the spectrum at approximate 530 nm (Fig. 7a). In the absence of biogenic amines, the addition of DFA/CS_2/Hg(II) to the Au NPs slightly induces a red shift of Au NPs maximal absorption band (Fig. 7b). By covalently conjugating Au NPs to the building blocks of cellulose-FPS/βCD through a stimuli-sensitive bond (e.g., a pH responsive bond), one is able to not only load Au NPs into cellulose-FPS/βCD but also control Au NPs release kinetics from the cellulose-FPS/βCD in an environmentally sensitive manner. However, in the presence of diethanolamine (DEA) as a biogenic amines and Hg^{2+} the absorbance of AuNPs at 530 nm decreased gradually and the absorbance at 690 nm mutually increased and the color changes from red to purple arising from the raction between Au NPs and Hg^{2+} (Fig. 7c).

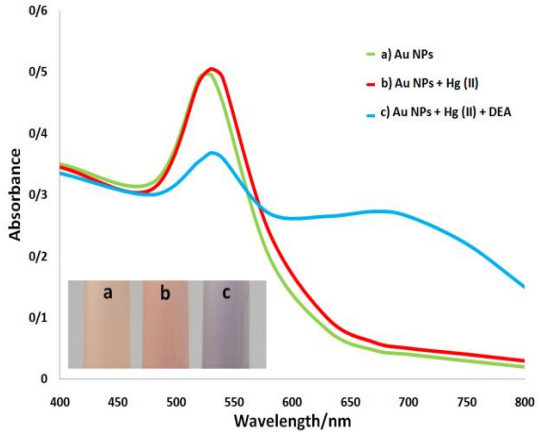

Fig. 7. Extinction spectra of different systems. (Inset were photos of different system).

The size details, particles shape, and surface morphology were investigated by FE–SEM, and TEM. Transmission electron microscope (TEM) and energydispersive X-ray (EDX) analysis were performed to character the change of morphology and composition of Au NPs before and after reaction. The as-prepared Au NPs were well-defined morphology with an average size of 30 nm and only Au element was measured (Fig. 8a). However, after of DFA/CS_2/Hg(II) and DEA were introduced, well-defined Au@Hg core−shell nanostructures larger in size than Au NPs could be observed (Fig. 8b and 8c). EDX analysis confirmed the coexistence of Au and mercury elements (Fig. 8d and 8e). The basic environment was pivotal for deposit mercury nanoshells on the surface of gold NPs. Hence, taking advantage of the weak basicity of biogenic amines, visual detection of they can be realized.

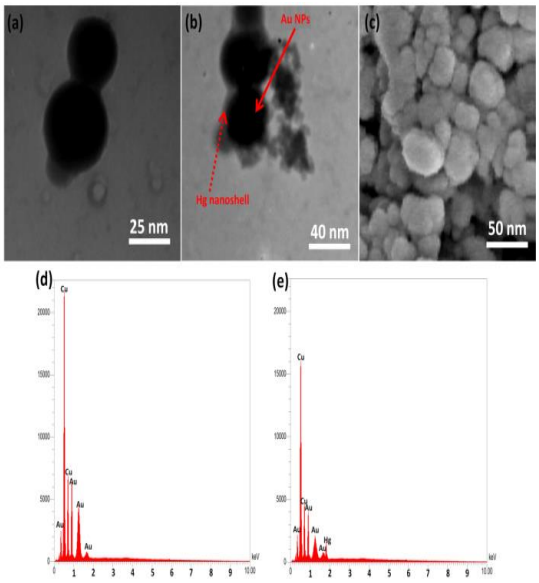

Fig. 8. TEM images of a) Au NPs before reaction; b) and after reaction; c) FE-SEM images of Au NPs after reaction; corresponding EDX results of d) Au NPs before reaction; e) and after reaction.

Result of reaction parameters on the blue shift of longitudinal LSPR peak of Au NPs was checked. As shown in Fig. 9, the blue shift of longitudinal LSPR peak was increased with the concentration of Hg (II) since higher concentration of Hg (II) was beneficial to produce more mercury metallization.

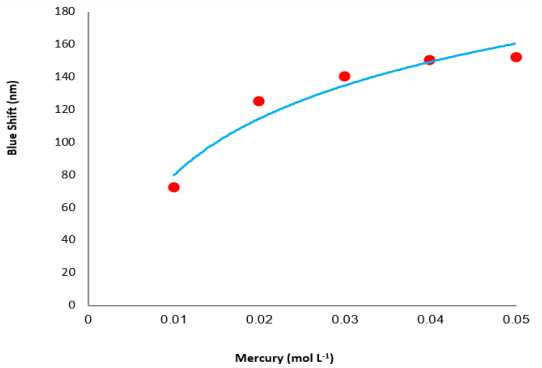

Fig. 9. Effect of concentration of mercury on the blue shift of longitudinal LSPR peak of Au NPs.

The blue shift of longitudinal LSPR peak was increased with increase of the DEA concentration and temperature (Fig. 10 and 11). Higher DEA concentration and temperature would accelerate the mercury metallization. This methods are very desirable for monitoring of food spoilage since for all perishable foods the spoilage flow generally will speed up to generate more biogenic amines at high temperatures [44].

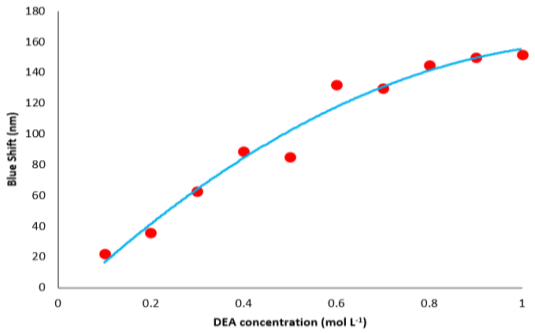

Fig. 10 Effect of concentration of DEA on the blue shift of longitudinal LSPR peak of Au NPs.

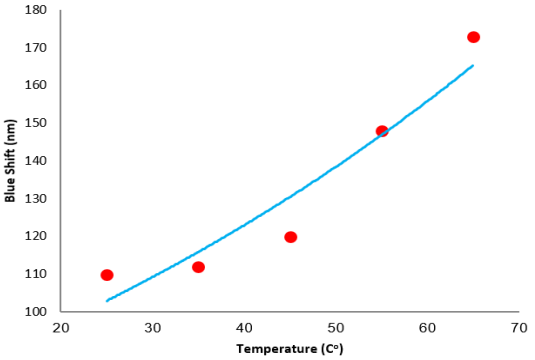

Fig. 11. Effect of temperatureon the blue shift of longitudinal LSPR peak of Au NPs.

We then quantified gold release kinetics from the cellulose-FPS/βCD at different pH values using ICP-MS. The gold release kinetics represents how fast the mgold leak out of the cellulose-FPS/βCD, plotted as the weight ratio of the accumulative released gold to the total gold payload against time. Fig. S6 showed the mercury release kinetics from the cellulose-FPS/βCD NPs at three distinct pH values, pH = 7.1, 9.7, and 11.4. The gold release rate from the cellulose-FPS/βCD at pH = 9.7 and 11.4 was significantly faster than at pH = 7.1. When the gold loading yield was 0.94 wt % (Fig. 12), it took the FPS/βCD/Au NPs around 80 and 100 second to release 70% of total mercury payload at pH = 9.7 and 11.4, respectively. The contrast of the gold release rate was even more sharper within the first a few seconds. For example, during the first 20 second period, 19 and 37% of the gold payload was released at pH = 9.7 and 11.4, respectively, while only 1% was released at pH = 7.1. These results suggest that gold release kinetics from the cellulose-FPS/βCD NPs is pH-dependent. Also, the rate of mercury metallization also showed pH-dependent. The rate was increased as pH rose from 8.5 to 11.7 due to the expediting the gold release rate from the cellulose-FPS/βCD NPs at high pH. However, when pH was higher than 12.0, the rate decreased on the contrary because of the formation of mercury hydroxide (Fig. 13).

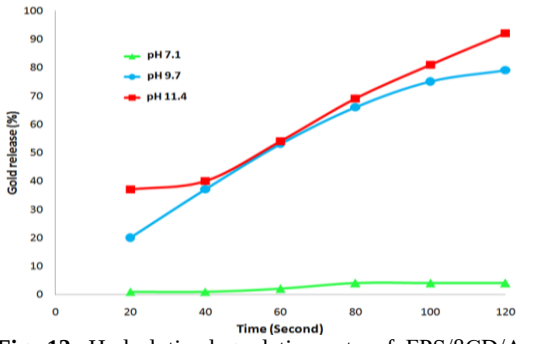

Fig. 12. Hydrolytic degradation rate of FPS/βCD/Au NPs at pH = 7.1, 9.7 and 11.4.

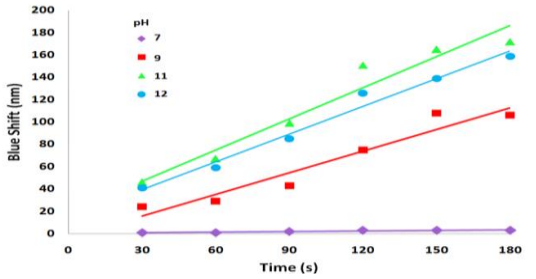

Fig. 13. Effect of pH the blue shift of longitudinal LSPR peak of Au NPs.

Colorimetric detection of biogenic amines was carried out with biogenic amine and TMA was used as a model biogenic amine because of its high vapor pressure. On adding of TMA methanol solution into the mixture of FPS/βCD/Au NPs, and DFA/CS_2/Hg(II), the longitudinal LSPR peak of Au NPs was blue-shifted with the incubation time and reached steady-state for about 180 second (Fig. 14). The testing efficiency responding to other biogenic amines were also examined. As shown in Fig. 15, the sensing system exhibited similar color change but with different sensitivity toward other common biogenic amines because of their different basicity.

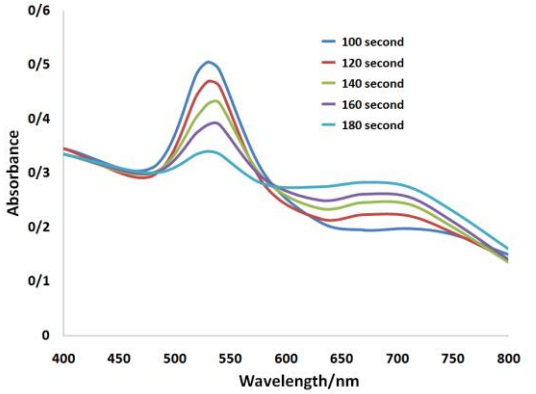

Fig. 14. Extinction spectra evolution of Au NPs solution on addition of TMA ethanol solution (12 mmol L^{-1}) into the mixture of FPS/βCD/Au NPs, and DFA/CS_2/Hg(II) NPs with the incubation time.

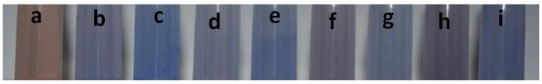

Fig. 15. Color evolutions of sensing system with the different biogenic amine (1.8 mmol L^{-1}) (a: blank, b: tyramine, c: histamine, d: β-phenylethylamine, e: spermine, f: trimethylamine, g: tryptamine, h: spermidine, i: cadaverine).

A 500 µL of TMA ethanol solution was added into the bottom of microcentrifuge tube without straight touching the sensor. Nano sensors were synthesized by solidifying FPS/βCD/Au NPs, and DFA/CS_2/Hg(II) NPs into agarose. Different concentrations of trimethylamine ethanol solutions were added into an enclosed microcentrifuge tube to mimick the spoilage of packaged food and allow trimethylamine vapor to permeate into the nano sensor. The concentration of trimethylamine steam would increase with the concentration of trimethylamine ethanol solution as well as the exposure time until trimethylamine steam reached saturation. Color change of sensor on presence to trimethylamine vapor was shown in Fig. 16. The sensors shows almost similar colors after exposure to different concentrations of trimethylamine vapor. It took about 10 min for the color development of nano sensor to achieve stabilization under high concentration of trimethylamine vapor.

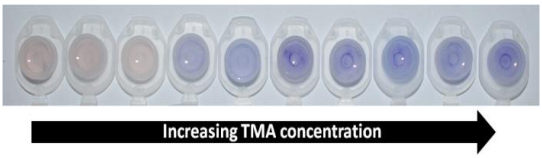

Fig. 16. Color evolutions of nano sensor on exposure to TMA vapor produced in an enclosed microcentrifuge tube containing 500 µL TMA ethanol solution at room temperature. The concentration of TMA ethanol solution (from left to right, mol L^{-1}) : 0, 3.62×10^{-4}, 1.97×10^{-3}, 3.75×10^{-3}, 1.23×10^{-2}, 2.09×10^{-2}, 2.98×10^{-2}, 4.06×10^{-2}, 0.124, 0.202, respectively.

The stability of nano sensor after stored at 3 and 28 °C for 24 days was investigated by exposure to the trimethylamine vapor. Compared to the new prepared nano sensors, the nano sensors almost did not change in color and showed similar sensing performance even after stored at 3 and 28 °C for 24 days. Therefore, the color change of nano sensor was stable and trustworthy for the diagnosis of volatile biogenic amines (Fig. 17). Finally, The proof of concept related with the performance of the labels were carried out with fresh meat and packaged in microcentrifuge tube. Nano sensor were added into an enclosed microcentrifuge tube to mimick the spoilage of packaged meat and allow trimethylamine vapor to penetrate into the nano sensor. The study was carried out at constant temperature, 3 and 28 ºC, respectively. The spoilage of the meat was accompanied by the darkening of the red nano sensors to purple, demonstrating that the material may encounter practical uses, for example, for visually informing the consumer of the freshness (Fig. 18).

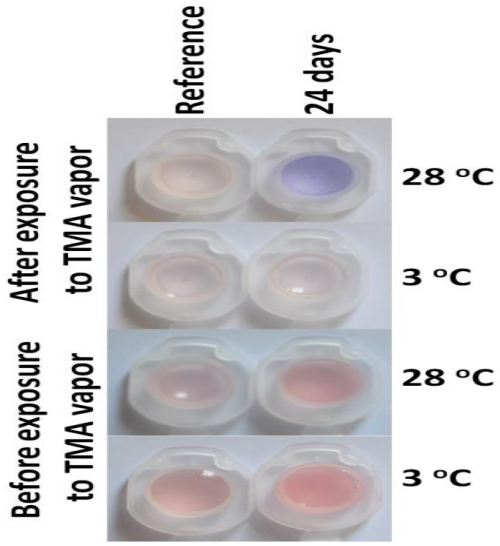

Fig. 17. The nano sensor was stored at 3 and 28 °C in the peresnt of 500 µL TMA ethanol solution (0.051 mol L^{-1}) without special precautions for 24 days.

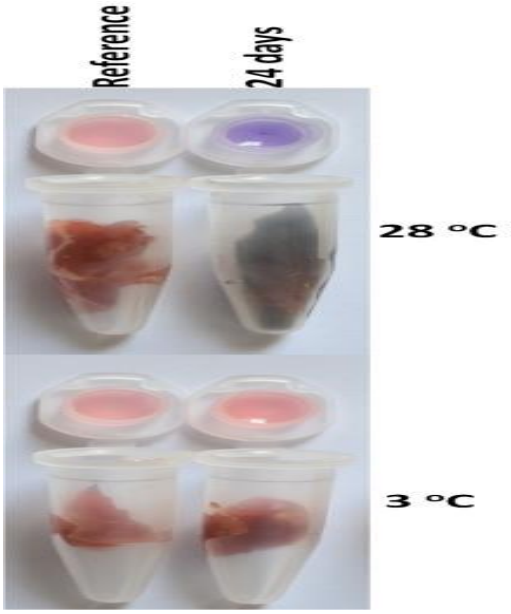

Fig. 18. Color development of nano sensor inside refrigerated (3 ºC) and room temperature (30 ºC) tray-packaged meat.

4. CONCLUSION

We have successfully presented a method for comfortable, nondestructive, free tool, and visual monitoring of biogenic amines. The color change of nano sensor was found to correlate with

biogenic amines generated, and enabling in situ monitoring of food spoilage. Hence, it is concluded that the nano sensor can be successfully utilised to predict the degree of spoilage in stored meat. We reported a hydrolysis-induced mercury metallization reaction by basic biogenic amines to tune the LSPR adsorption peak of gold NPs. In comparison with antecedent offered methods for the detection of biogenic amines to monitor food spoilage, this method has been many advantages. This sensor provided an instrument-free, sensitive, and high resolution colorimetric method for the end-users due to the distinctive multiple color readout. Also, this sensor was simple to fabricate by only using Au NPs as the signal transducer, the design of array sensors was not necessary for different biogenic amines and the detection of biogenic amines was nondestructive, no pretreatment was needed. Finally, without the usage of bioenzymes, this sensor was cost-effective and robust for practical application.

REFRENCESE

[1] J.L. Pablos, M. Trigo-Lopez, F. Serna, F.C. Garcia and J.M. Garcia, Solid polymer substrates and smart fibres for the selective visual detection of TNT both in vapour and in aqueous media, *RSC Adv.* 4 (2014) 25562–25568.

[2] K. Galic, M. Scetar and M. Kurek, The benefits of processing and packaging, *Trends Food Sci. Technol.* 22 (2011) 127–137.

[3] S.F. Schilthuizen, Communication with your packaging: possibilities for intelligent functions and identification methods in packaging, *Packag. Technol. Sci*. 12 (1999) 225–228.

[4] B. Kuswandi and Y. Wicaksono, Smart packaging: sensors for monitoring of food quality and safety, *Sens. Instrum. Food Qual. Saf.* 5 (2011) 137–146.

[5] D. Restuccia, U.G. Spizzirri, O.I. Parisi, G. Cirillo, M. Curcio, F. Iemma, F. Puoci, G. Vinci and N. Picci, New EU regulation aspects and global market of active and intelligent packaging for food industry applications, *Food Control*. 21 (2010) 1425–1435.

[6] A. Pacquit, J. Frisby, D. Diamond, K.T. Lau, A. Farrell, B. Quilty and D. Diamond, Development of a smart packaging for the monitoring of fish spoilage, *Food Chem.* 102 (2007) 466−470.

[7] P.Q. Leng, F.L. Zhao, B.C. Yin, B.C. Ye, A novel, colorimetric method for biogenic amine detection based on arylalkylamine N-acetyltransferase, *Chem. Commun*. 51 (2015) 8712−8714.

[8] J.L. Pablos, S. Vallejos, A. Munoz, M.J. Rojo, F. Serna, F.C. Garcia and J.M. Garcia, Solid polymer substrates and coated fibers containing 2,4,6-Trinitrobenzene motifs as smart labels for the visual detection of biogenic amine vapors, *Chem. Eur. J.* 21 (2015) 8733 – 8736.

[9] X.W. Huang, X.B. Zou, J.Y. Shi, Y. Guo, J.W. Zhao, J. Zhang and L. Hao, Determination of pork spoilage by colorimetric gas sensor array based on natural pigments, *Food Chem*. 145 (2014) 549−554.

[10] Z. Gao, K. Deng, X.D. Wang, M. Miró and D. Tang, High-resolution colorimetric assay for rapid visual readout of phosphatase activity based on gold/silver core/shell nanorod, *ACS Appl. Mater. Interfaces* 6 (2014) 18243−18250.

[11] X. Yang and Z. Gao, Enzyme-catalysed deposition of ultrathin silver shells on gold nanorods: a universal and highly efficient signal amplification strategy for translating immunoassay into a litmus-type test, *Chem. Commun.* 51 (2015) 6928−6931.

[12] Z. Zhang, Z. Chen, S. Wang, F. Cheng and L. Chen, Iodine-mediated etching of gold nanorods for plasmonic ELISA based on colorimetric detection of alkaline phosphatase, *ACS Appl. Mater. Interfaces* 7 (2015) 27639−27645.

[13] J. Chen, A.A. Jackson, V.M. Rotello and S.R. Nugen, Colorimetric Detection of Escherichia coli Based on the Enzyme-Induced Metallization of Gold Nanorods, *Small* 12 (2016) 2469−2475.

[14] T. Lin, Y. Wu, Z. Li, Z. Song, L. Guo and F. Fu, Visual monitoring of food spoilage based on hydrolysis-induced silver metallization of au nanorods, *Anal. Chem*. 88 (2016) 11022−11027.

[15] I.H. Cho, L. Mauer and J. Irudayaraj, In-situ fluorescent immunomagnetic multiplex detection of foodborne pathogens in very low numbers, *Biosens. Bioelectron*. 57 (2014) 143−148.

[16] G. Olafsdottir, R. Jonsdottir, H.L. Lauzon, J. Luten and K.J. Kristbergsson, Characterization of Volatile Compounds in Chilled Cod (Gadus morhua) Fillets by Gas Chromatography and Detection of Quality Indicators by an Electronic Nose, *Agric. Food Chem*. 53 (2005) 10140−10147.

[17] J.R. Askim, M. Mahmoudi and K.S. Suslick, Optical sensor arrays for chemical sensing:

the optoelectronic nose, *Chem. Soc. Rev*. 42 (2013) 8649−8682.

[18] R.A. Potyrailo, N. Nagraj, Z. Tang, F.J. Mondello, C. Surman and W.J. Morris, Battery-free radio frequency identification (RFID) sensors for food quality and safety, *Agric. Food Chem*. 60 (2012) 8535−8543.

[19] K. Sowoidnich, H. Schmidt, H.D. Kronfeldt and F. Schwägele, A portable 671 nm Raman sensor system for rapid meat spoilage identification, *Vib. Spectrosc*. 62 (2012) 70−76.

[20] S. Sen and P. Sarkar, A novel third-generation xanthine biosensor with enzyme modified glassy carbon electrode using electrodeposited MWCNT and nanogold polymer composite film, RSC Adv. 5 (2015) 95911−95925.

[21] L.D. Bonifacio, G.A. Ozin and A.C. Arsenault, Photonic nose–sensor platform for water and food quality control, *Small* 7 (2011) 3153−3157.

[22] M.K. Morsy, K. Zór, N. Kostesha, T.S. Alstrøm, A. Heiskanen, H. El-Tanahi and A. Sharoba, Development and validation of a colorimetric sensor array for fish spoilage monitoring, *Food Control* 60 (2016) 346−352.

[23] M.S. Steiner, R.J. Meier, A. Duerkop and O. Wolfbeis, Chromogenic sensing of biogenic amines using a chameleon probe and the red− green− blue readout of digital camera images, *Anal. Chem*. 82 (2010) 8402−8405.

[24] F. B. Erim, Recent analytical approaches to the analysis of biogenic amines in food samples, TrAC, *Trends Anal. Chem*. 52 (2013) 239−247.

[25] P.Q. Leng, F.L. Zhao, B.C. Yin and B.C. Ye, A novel, colorimetric method for biogenic amine detection based on arylalkylamine N-acetyltransferase, *Chem. Commun*. 51 (2015) 8712−8714.

[26] M. Gao, S. Li, Y. Lin, Y. Geng, X. Ling, L. Wang, A. Qin and B.Z. Tang, Fluorescent Light-Up detection of amine vapors based on aggregation-induced emission, ACS Sens. 1 (2016) 179−184.

[27] S.F. Liu, A.R. Petty, G.T. Sazama and T.M. Swager, Single-walled carbon nanotube/metalloporphyrin composites for the chemiresistive detection of amines and meat spoilage, *Angew. Chem., Int. Ed*. 54 (2015) 6554−6557.

[28] S. Rochat and T.M. Swager, Fluorescence sensing of amine vapors using a cationic conjugated polymer combined with various anions, *Angew. Chem., Int. Ed*. 53 (2014) 9792−9796.

[29] T. Ramon-Marquez, A.L. Medina-Castillo, A. Fernandez-Gutierrez and J.F. Fernandez-Sanchez, Novel optical sensing film based on a functional nonwoven nanofibre mat for an easy, fast and highly selective and sensitive detection of tryptamine in beer, *Biosens. Bioelectron*. 79 (2016) 600−607.

[30] Y.F. Huang, C.K. Chiang, Y.W. Lin, K. Liu, C.C. Hu, M.J. Bair and H.T. Chang, Capillary electrophoretic separation of biologically active amines and acids using nanoparticle-coated capillaries, *Electrophoresis* 29 (2008) 1942−1951.

[31] Z. Wang, F. Liu and C. Lu, Evolution of biogenic amine concentrations in foods through their induced chemiluminescence inactivation of layered double hydroxide nanosheet colloids, *Biosens. Bioelectron*. 60 (2014) 237−243.

[32] C.F. Chow, M.H. Lam and W.Y. Wong, Design and synthesis of heterobimetallic Ru (II)–Ln (III) complexes as chemodosimetric ensembles for the detection of biogenic amine odorants, *Anal. Chem*. 85 (2013) 8246−8253.

[33] R. Grau, A.J. Sánchez, J. Girón, E. Iborra, A. Fuentes and J.M. Barat, Nondestructive assessment of freshness in packaged sliced chicken breasts using SW-NIR spectroscopy, *Food Res. Int*. 44 (2011) 331−337.

[34] A.C. Manetta, L. Di Giuseppe, R. Tofalo, M. Martuscelli, M. Schirone, M. Giammarco and G. Suzzi, Evaluation of biogenic amines in wine: determination by an improved HPLC-PDA method, *Food Control* 62 (2016) 351−356.

[35] N. Gandhi, A. Kumar, C. Kumar, N. Mishra, P. Chaudhary, N.K. Kaushikd and R. Singh, Synthesis, characterization, thermal and biological activity of some novel Cadmium (II)–pyridine and purine base complexes, *Main Group Chem.* 15 (2016) 35–46.

[36] M. Zahedifar, A. Es-haghi, R. Zhiani and S.M. Sadeghzadeh, Synthesis of benzimidazolones by immobilized gold nanoparticles on chitosan extracted from shrimp shells supported on fibrous phosphosilicate, *RSC Adv*. 9 (2019) 6494–6501.

[37] M. Banach, Z. Kowalski, Z. Wzorek and K. Gorazda, A chemical method of the production of" heavy" sodium tripolyphosphate with the high content of Form I or Form II, *Pol. J. Chem. Techno*. 11 (2009) 13-20.

[38] Ph. Massiot, M.A. Centeno, I. Carrizosa and J.A. Odriozola, Thermal evolution of sol–gel-

obtained phosphosilicate solids (SiPO), *J. Non-Cryst. Solids* 292 (2001) 158-166.
[39] M. Stan, A. Vasdilescu, S. Moscu and M. Zaharescu, IR spectrometry study of the gels in the SiO_2-P_2O_5 system, *Rev. Roum. Chim*. 43 (1998) 425-432.
[40] H.S. Liu, T.S. Chin and S.W. Yung, FTIR and XPS studies of low-melting PbO-ZnO-P_2O_2 glasses, *Mater. Chem. Phys*. 50 (1997) 1-10.
[41] I.N. Chakraborty and R.A. Condrate, The vibrational spectra of glasses in the Na_2O-SiO_2-P_2O_5 system with a 1:1 SiO_2:P_2O_5 molar ratio, *Phys. Chem. Glasses* 26 (1985) 68-73.
[42] Y.K. Kim and R.E. Tressler, Microstructural evolution of sol-gel-derived phosphosilicate gel with heat treatment, *J. Mater. Sci*. 29 (1994) 2531-2535.
[43] G. Lakshminarayana and M. Nogami, Proton conducting organic–inorganic composite membranes under anhydrous conditions synthesized from tetraethoxysilane/methyltriethoxysilane/trimethyl phosphate and 1-butyl-3 methylimidazolium tetrafluoroborate, *Solid State Ionics* 181 (2010) 760-766.
[44] C. Zhang, A.X. Yin, R. Jiang, J. Rong, L. Dong, T. Zhao, L.D. Sun, J. Wang, X. Chen and C.H. Yan, Time–Temperature indicator for perishable products based on kinetically programmable Ag overgrowth on Au nanorods, *ACS Nano* 7 (2013) 4561−4568.